Accepted Manuscript

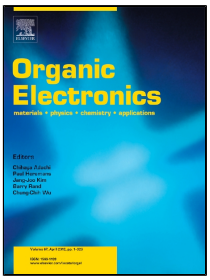

Perovskite Photo-Detectors (PVSK-PDs) for Visible Light Communication

Luigi Salamandra, Narges Yaghoobi Nia, Melania Di Natali, Claudio Fazolo, Silvia Maiello, Luca La Notte, Gianpaolo Susanna, Angelo Pizzoleo, Fabio Matteocci, Lucio Cinà, Leonardo Mattiello, Francesca Brunetti, Aldo Di Carlo, Andrea Reale

PII:	S1566-1199(19)30109-0
DOI:	10.1016/j.orgel.2019.03.008
Reference:	ORGELE 5146
To appear in:	*Organic Electronics*
Received Date:	27 September 2018
Accepted Date:	06 March 2019

Please cite this article as: Luigi Salamandra, Narges Yaghoobi Nia, Melania Di Natali, Claudio Fazolo, Silvia Maiello, Luca La Notte, Gianpaolo Susanna, Angelo Pizzoleo, Fabio Matteocci, Lucio Cinà, Leonardo Mattiello, Francesca Brunetti, Aldo Di Carlo, Andrea Reale, Perovskite Photo-Detectors (PVSK-PDs) for Visible Light Communication, *Organic Electronics* (2019), doi: 10.1016/j.orgel.2019.03.008

Perovskite Photo-Detectors (PVSK-PDs) for Visible Light Communication

Luigi Salamandra[a,b,c,§], Narges Yaghoobi Nia[b,c], Melania Di Natali[c], Claudio Fazolo[c], Silvia Maiello[c], Luca La Notte[b,c], Gianpaolo Susanna[a,b,c], Angelo Pizzoleo[a,c], Fabio Matteocci[b,c], Lucio Cinà[b,c,d], Leonardo Mattiello[e], Francesca Brunetti[b,c],Aldo Di Carlo[b,c], Andrea Reale[b,c,*]

a. ISCOM - Istituto Superiore delle Comunicazioni e delle Tecnologie dell'Informazione - Ministero dello Sviluppo Economico, Viale America 201, 00144 Rome, Italy
b. CHOSE - Centre for Hybrid and Organic Solar Energy - University of Rome "Tor Vergata", Via del Politecnico 1, 00133 Rome, Italy
c. Department of Electronics Engineering - University of Rome "Tor Vergata", Via del Politecnico 1, 00133 Rome, Italy
d. Cicci Research srl, Via Giordania 227 - 58100 Grosseto
e. Department of Basic and Applied Sciences for Engineering - University of Rome "La Sapienza", Via del Castro Laurenziano 7, 00161 Rome, Italy
* *reale@ing.uniroma2.it*
§ *luigi.salamandra.ext@mise.gov.it*

Abstract

Visible Light Communication technology has the potential to become a leading actor in the future 5G network, thanks to features such as efficient "re-use of re-sources", native privacy security and human safeness (compared to radio-frequency applications). Among the several configurations achievable to realize a VLC link, the use of innovative photovoltaic devices as receiver, based on organic-inorganic printable semiconductors (hybrid perovskite materials), has the potential to pave the way to new scenario applications, thanks to the inherent cheaper costs of fabrication via roll-to-roll solution-based processes, possibly on flexible substrates. In this context, we have fabricated photo-detectors with three different types of perovskite, and used with a commercial cool-white LED to realize a prototype of visible light communication data link. Using a single-stage trans-impedance amplifier for the perovskite photodetector, we have reached a remarkable frequency bandwidth close to ~800KHz.

Keywords

Perovskite photovoltaics, photodetector bandwidth, visible light communication, 5G.

1. Introduction

The rapid growth of data traffic over wireless infrastructures (video and audio streaming, file sharing, data and even voice over internet), together with the lack of available radio-frequency (RF) spectrum, will be the bottle-neck for high-speed data transmission in the near future. However, thanks to the novel approach of an intelligent and shared use of "resources" (introduced by Smart City and 5G network concepts) [1,2], a possible solution is to introduce new communication technologies, that could work in a complementary manner to the pre-existent network infrastructures, and maybe grant new services and application scenarios.

This is the case of visible light communication (VLC), a subset of optical wireless communication (OWC) technologies: VLC principle is the use of artificial light sources in the visible range (between 380 and 780nm), both as illumination and data media [3,4], thanks to a direct modulation of the current faster than the human eye perception of a flicker [5]. Such vast unregulated frequency spectrum (400÷800 THz), currently license-free, makes VLC a technology with very attractive capabilities [6], thanks to: a) energy efficiency (coupling to indoor illumination); b) inherent "safety" with respect to environments where RF-based technologies are prohibited or strictly regulated (such as hospitals, gas stations and airplanes); c) underwater data links availability; d) "security" of light as medium (the signal could not be intercepted over walls, like in radio frequency transmissions) [7,8].

VLC isn't a new concept in the field of telecommunications. Since the year 2000, Twibright Labs developed the RONJA project [9], in which a Tx/Rx (transmitter/receiver) station based on ultra-bright high-power red light emitting diodes was demonstrated. As reported in the website project [http://ronja.twibright.com/about.php] "*Ronja (Reasonable Optical Near Joint Access) is an User Controlled Technology (like Free Software) project of optical point-to-point data link. The device has 1.4km range and has stable 10Mbps full duplex data rate*" (cit.).

The most appealing property of VLC is the use of ordinary lamps (instead of dedicated communication devices) to transmit signals over *short distances*. At the beginning, VLC using fluorescent lamps (10kb/s) [5] couldn't be a reliable technology, but thanks to the developments in solid-state lighting (SSL), in particular highly efficient white light-emitting diodes (White-LEDs), with longer life span and much higher power efficiency than conventional lamps, data link over 500Mb/s have been demonstrated [10], and this has permitted to consider VLC more than "science fiction". Nowadays, there is an on-going IEEE standardization [11,12], speaking of a data rate up to 3.5Gb/s [13], and state-of-the-art data links have been reported with transmission speed over 10Gb/s [14] using a WDM (Wavelength Division Multiplexing) approach with RGB (Red + Green + Blue) LEDs.

A relevant segment in the VLC field is focused more on low cost innovative devices, in particular on the Rx-side of the data link, rather than "light source" and "fast speed". Many groups are studying the use of new generation Photo-Voltaic (PV) technologies (coming from solar energy harvesting research activities and knowhow) applied to telecommunication. Among them, in the past few years, PV technologies based on organic–inorganic hybrid perovskite materials have demonstrated remarkable progress [15–20]. Extensive research efforts have been undertaken to improve the Power Conversion Efficiency (PCE) of Perovskite Solar Cells (PVSK-SCs) from less than 4% [21] to more than 22.7% [22] in less than a decade. In addition to very high efficiencies, PVSK-SCs present opportunities to markedly reduce manufacturing costs due to ease of processing via various solution-based, low-temperature deposition methods [23–25] and the potential for roll-to-roll manufacturing on flexible substrates [26], thus permitting for instance wearable devices [27]. Moreover, preliminary life-cycle assessments show that perovskite solar modules are expected to have lower environmental impact [28–31], and the important energy payback time (EPBT) metric has been calculated to be shorter for PVSK-SCs in comparison to other more established PV technologies [32].

In this manuscript we propose the study of a perovskite-based photovoltaic device use in photodetector (PVSK-PD) mode (reverse bias) [33,34]. Three perovskite formulations containing single cation lead iodide, double cation/halide and triple cation double halide, respectively, were employed in the fabrication of mesoscopic structured devices using sequential deposition method in ambient condition (out of an inert atmosphere, like in a glove-box). The different perovskite layers, deposited with the same deposition method (double-step), were characterized with UV-VIS (Ultraviolet-Visible) absorbance, whereas the 10mm^2 (active area) PVSK-PDs were tested with Photoluminescence (PL) and photovoltaic performance analysis methods, like I-V and Responsivity measurements (see Experimental section for details). Then, the best device was inserted in a complete Tx/Rx setup and tested as photo-detector in a prototype of VLC data link.

2. Experimental

2.1 Materials

PbI_2 and $PbBr_2$ were purchased from TCI company, while MAI, FAI and MABr from Dyesol. Spiro-OMeTAD was produced by Borun. All the solvents (IPA anhydrous, DMF and DMSO) come from Sigma-Aldrich.

2.2 Fabrication

Transparent substrate (FTO)

A raster scanning laser (Nd:YVO_4 pulsed at 30kHz average output power of 10W) was used for patterning the FTO/glass substrates (Pilkington, 15Ω/□, 25x25mm^2). The substrates were cleaned in an ultrasonic bath, using detergent cleaning solution in de-ionized water, de-ionized water and 2-propanol (10min each step), respectively.

Electron transport layer (c-TiO_2+m-TiO_2)

A compact TiO_2 (c-TiO_2) layer was deposited onto the patterned FTO by Spray Pyrolysis Deposition using a previously reported procedure [35]. Precursor spray solution consisted of 0.16M Diisopropoxytitanium bis acetylacetonate and 0.4M Acetylacetone in ethanol. A mesoporous TiO_2 (m-TiO_2) layer (18NR-Tpaste, Dyesol), diluted with ethanol, ratio of 1:5 (w/w), was spin coated onto the c-TiO_2 surface, at 1500rpm for 20sec, then sintered using a standard thermal annealing procedure [19].

Perovskite active layer

$MAPbI_3$ (single-cation): the perovskite layer was deposited via double step deposition method, using crystal engineering approach [35]. Briefly, a supersaturated solution of PbI_2 in DMF, made dissolving 535mg of PbI_2 in 1ml of DMF, was deposited by spin-coating at 6000rpm for 10sec. The small area devices were annealed from RT (room temperature) to 40°C in 1min, keeping last temperature for 2min, and then the temperature was elevated to 60°C for 1min, and remained at this temperature for 1min more. In the next step, the cooled PbI_2(DMF) layers were dipped in a solution of methyl-ammonium iodide (CH_3NH_3I in anhydrous 2-propanol 10mg/ml) for 10min at room temperature. Then the devices were washed immediately with 2-propanol by spin-coating at 6000rpm for 10sec. Finally, the devices were annealed from room temperature to 70°C in 1min, keeping at 70°C for 2min, then elevating from 70°C to 115°C in 3min and remaining for 4min at this temperature.

(FA/MA)Pb(I/Br) (double-cation): the PbX_2 films were prepared by consecutive two-step spin-coating process with a solution of 1.2M (85:15 molar ratio of PbI_2:$PbBr_2$) in DMF/DMSO (90/10 v/v) mixture. The films were annealed at 70°C for 10min. After cooling to RT, the film was exposed to FAI and MABr (85:15 molar ratio) mixture in isopropanol for 90sec, then the film was spun and annealed at 100°C for 30min.

(FA/MA/Cs)Pb(I/Br) (triple-cation): regarding the fabrication of a triple-cation perovskite layer, in the initial PbX_2 solution we added 5% of CsI, whereas the deposition procedure still remain the same previously descripted for the double-one.

Hole transport layer (Spiro-OMeTAD) and counter electrode (Au)

A 73.2mg/ml solution of 2,20,7,70-tetrakis-(N,N-dip-methoxyphenylamine)9,9'-spirobifluorene (Spiro-OMeTAD) was deposited by spin coating at 2000rpm for 20sec. The Spiro-OMeTAD precursors were purchased from Sigma-Aldrich and Merck companies, respectively. The Spiro-OMeTAD solution was doped with 26.8µl of tert-butylpyridine (TBP), 16.6µl of Lithium Bis(Trifluoromethanesulfonyl)Imide (Li-TFSI) solution (520mg in 1ml of acetonitrile) and 7.2µl of cobalt 209 (stock solution 375mg in 1ml of acetonitryl). Finally, the prepared samples were introduced into a high vacuum chamber (10^{-6}mbar) to thermally evaporate Au back contacts (thickness ~80nm).

2.3 Characterization

The devices were characterized in photo-conductive mode using a Keithley 2602B Source-Meter Unit (SMU) and a cool-white LED of Lumiled (Philips). The LED power was measured using a calibrated FDS100 Si photodetector (250-1000nm, rise/fall-time of 13ns), from Thorlabs. Same photodetector was also used in the set-up for Time-Response (Bandwidth and Eye-Diagram); the set-up involves also a self-made driving circuit for the light source and a wide-band Melles-Griot trans-impedance amplifier, optimized up to 20MHz (fixed gain). The set-up is used also as VLC link (without modification). The devices in photo-voltaic mode were tested under a solar simulator (ABET Sun 2000, class A) with AM1.5G filter at 1sun (100mW/cm^2) illumination conditions, calibrated with a certified reference Si-cell (RERASolutions RR-1002). Responsivity analysis was performed with a commercial apparatus, Arkeo from Cicci Research s.r.l., based on a 300 Watts Xenon lamp monochromatic light (300÷1100nm), a source meter and a thermal controlled stage. The same stage allowed to monitor, through a fiber-based spectrometer, the Photo-Luminescence signal of the devices, excited by a green (532nm) laser at 45° of incidence with a circular spot diameter of 1mm. All the set-ups are controlled remotely with a LabVIEW interface.

3. Results & Discussion

We realized photovoltaic devices with 3 different types of Perovskite, (*i*) single cation $MAPbI_3$ (from now on identified as MAPI-1), (*ii*) double cation *(FA/MA)Pb(I/Br)* (as FAMA-2), and (*iii*) triple cation *(FA/MA/Cs)Pb(I/Br)* (as CsFAMA-3), leaving unchanged the other layers of the architecture and active area (see Experimental section for details). In such way, we compare the different performances of the perovskite-based photodetectors only with respect to the perovskite active layer composition (Figure 1).

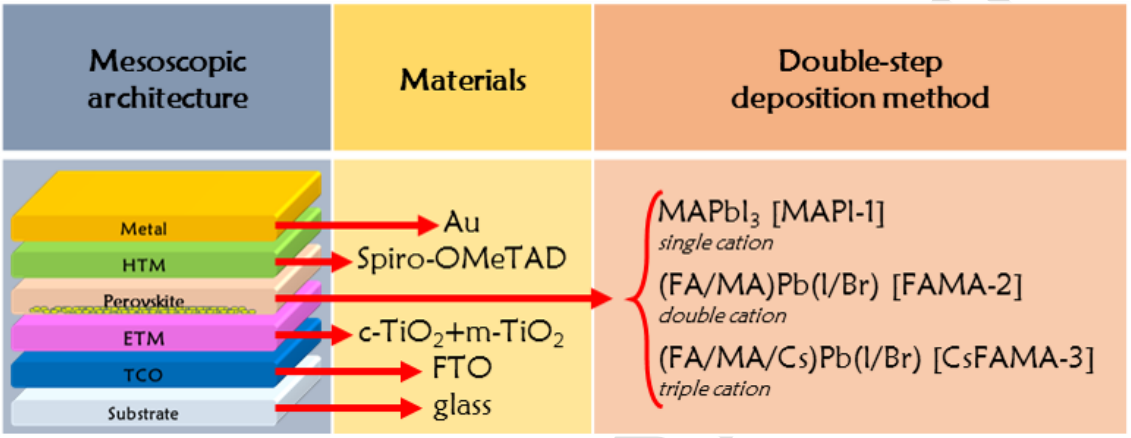

Figure 1. Schematic of the device architecture; the 3 devices are nominally equal, except for the perovskite material used for the realization of the active layer.

3.1 Photo-Voltaic and -Conductive behaviours

Firstly, we have characterized the current (density) versus voltage dependence (J-V) performance of the devices in photo-voltaic mode (as solar-cell), evaluated under AM1.5G solar illumination (1sun)**Error! Reference source not found.**. The best photo-conversion efficiencies collected from single-, double- and triple-cation devices were around 15.9, 16.4 and 17%, respectively. The change from single- to triple-cation structure leads to improve the overall performance of the device (all the parameters, V_{OC}, J_{SC} and FF, increased). Figure 2**Error! Reference source not found.** shows a couple of J-V curves for each device type, due to the well-known problem affecting the perovskite-based photovoltaic technology, *hysteresis* [36–38]. As evident, the CsFAMA-3 suffers sensibly less the hysteresis effect; for example, taking into account the difference between open circuit voltage values (ΔV_{hyst}) registered in forward and reverse potentiostatic scan direction (scan rate S_R fixed at 25mV/sec), it appears evident that the triple-cation present not only better PV performances, but also a reduction of the device hysteresis (decrease the "hysteric delay time", $\boldsymbol{\tau}_{hyst}$, defined as $\Delta V_{hyst} / S_R$). The main parameters of the devices are reported in Table 1.

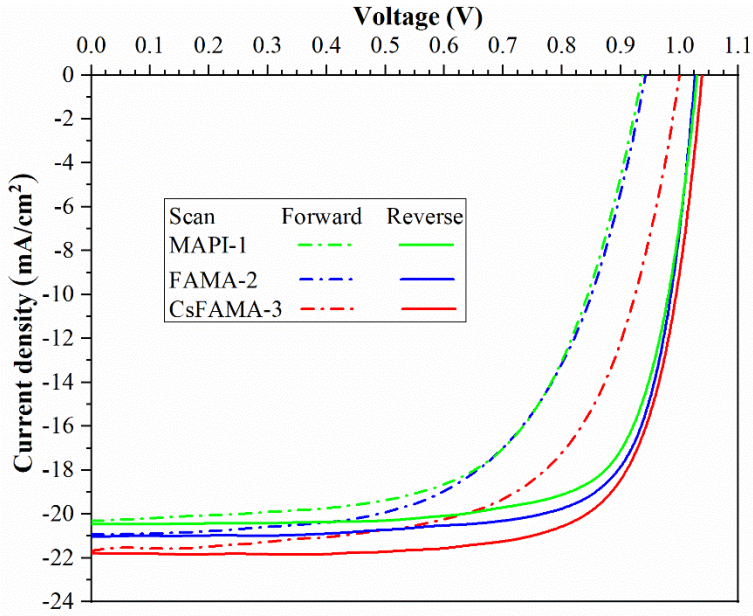

Figure 2. J-V curves of the 3 perovskite-based devices, under illumination of 100mW/cm² (AM1.5G). The line type indicates the potentiostatic scan direction used to measure the J-V: (dash) forward, (continuous) reverse. The scan rate was always 25mV/sec.

Device	Scan	V_{OC} (V)	J_{SC} (mA/cm²)	FF (%)	PCE (%)	ΔV_{hyst} (mV)	S_R (mV/sec)	τ_{hyst} (sec)
MAPI-1	reverse	1.034	20.33	75.6	15.89	96	25	3.84
	forward	0.938	20.33	57.9	11.04			
FAMA-2	reverse	1.032	21.01	75.7	16.41	88		3.52
	forward	0.944	21.03	57.2	11.36			
CsFAMA-3	reverse	1.043	21.69	75.2	17.01	39		1.56
	forward	1.004	21.89	61.1	13.43			

Table 1. Electrical parameters extracted from J-V measures for the 3 different perovskite solar cells.

The same devices were also measured in photo-conductive mode (as photo-detector), estimating from the current versus voltage dependence (I-V) both rectifying effect (dark condition), and current gain (photo-current) produced under 10mW/cm² illumination of a Cool-White LED (CW) at negative bias (Figure 3). MAPI-1 and FAMA-2 show similar behaviours in dark and light conditions; in particular, considering the dark one, both devices suffer of the same important hysteresis effect, as highlighted from the cusp point of the curve shifted over 500mV with respect to the ideal [0V|0A] central point. Under 10mW/cm² light power from the CW, the MAPI-1 exhibits a larger photo-current and V_{OC} (~800mV) with respect to FAMA-2, but basically the two devices are comparable. Instead, the CsFAMA-3 has a less decentralized cusp point in dark condition, and this means a less hysteresis of the device [39]. Moreover, under the CW light, it shows a photo-current comparable to the FAMA-2, and a larger V_{OC} (~1V). Furthermore, only for the CsFAMA-3 case, we have measured the I-V under other CW illumination levels, 0.1 and 1mW/cm², finding a good linear

agreement between light power and photo-current. The on/off switching ratio ($I_{on/off}$) of the photodetectors between dark and light current are reported in Table 2.

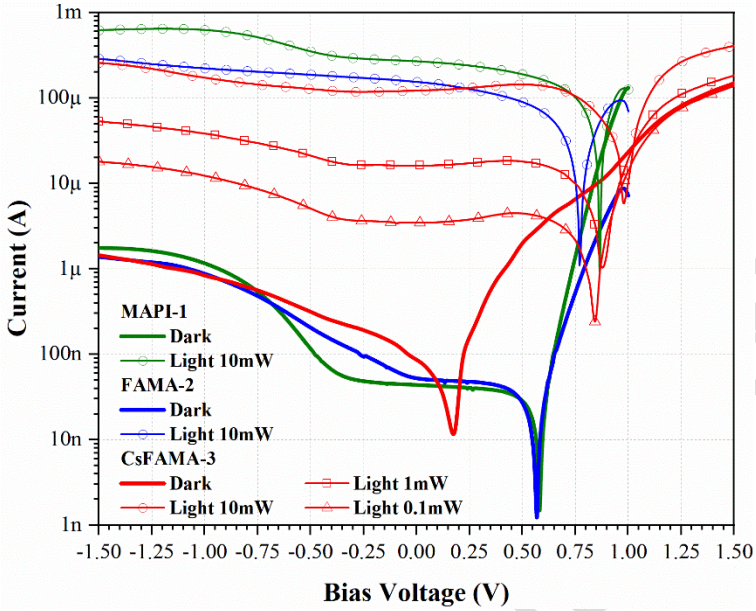

Figure 3. I-V behaviour of the PVSK-PDs under several illumination conditions of a Cool-White LED. The I-V measures were performed in reverse scan, 25mV/sec, both dark and light.

3.2 Frequency Bandwidth

The three perovskite-based devices were evaluated in terms of frequency bandwidth (Figure 4). Due to the known problem of the PVSK technology, accelerating its ageing at strong negative bias [38], and considering that all the devices show an optimal gain current in the range (-0.5÷0)V (see Figure 3), a low negative bias, equal to -100mV, was chosen as measure condition. For each bandwidth curve, the 0dB reference value was attributed considering the level states due to a "continuous" illumination condition, either dark (*low* level, LED switched-off) or light (*high* level, LED switched-on at 20mW/cm^2). The devices are evaluated including the effect of the active set-up (trans-impedance amplifier, TIA) described in the Experimental section (due to a limitation of the oscilloscope used in the experiment).In Figure 4, we reported also the bandwidth of the Cool-White LED, used as transmission source, and of the TTL driving signal used to modulate directly the CW itself, as comparison.

Firstly, it is notable how the three types of perovskite differ completely in frequency: MAPI-1 shows practically a monotone behaviour, and already before 1KHz its frequency response starts to decrease, reaching the cut-off frequency (f_{off}) at -3dB near 270KHz (268KHz). FAMA-2 remains practically stable up to 100KHz, and then a rapid decrease of the frequency response (f_{off} =584KHz) is observed. CsFAMA-3 shows the best performance, thanks to an initial increase in output signal gain (after 100Hz), that is maintained until ~500KHz; even if the frequency response drops fast at

higher frequencies (as FAMA-2), nevertheless the device could reach a remarkable cut-off frequency of ~800KHz (798KHz).

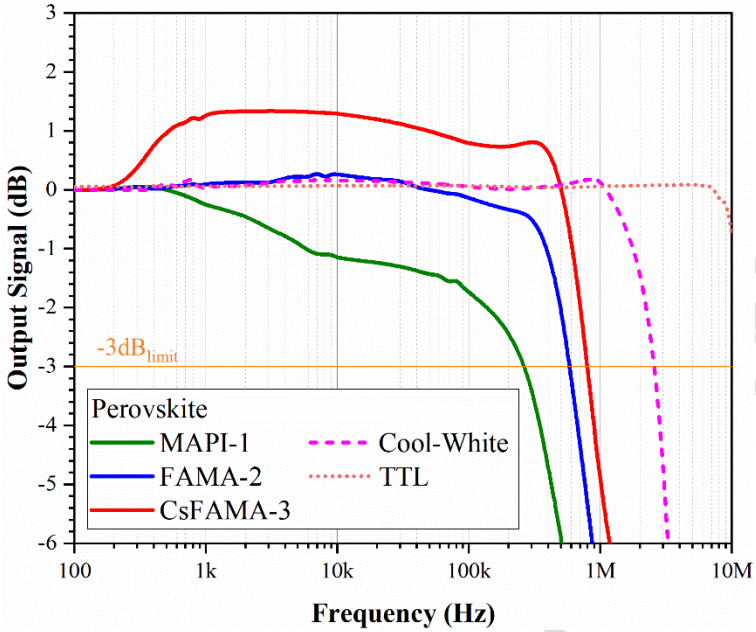

Figure 4. Bandwidths evaluated for the 3 different PVSK-PDs, polarized with a low negative bias (next to 0V); they are compared also with the ones of both transmitted optical signal (CW) and driving electrical source (TTL).

Which is the cause for such different time dependent behaviour? The devices have same structure, apart from the perovskite composition. The reduced hysterical behaviour of the CsFAMA-3 is a possible reason, determining a faster response to the time dependent optical stimulus. In fact, hysteresis behaviour comes from the limitation of the device to rapidly follow the electrical perturbation due to the voltage scan rate [37,38], with respect to a fixed illumination condition. In an analogue manner, at a fixed electrical bias, the time dependent optical perturbation induced by the LED modulation on the perovskite photo-detector determines a photo-response that is correlated to the same hysteresis phenomenon (device dependent). This means that the triple-cation device presenting the least hysteresis, reacts in the fastest way, thus showing the highest f_{off} of 793KHz.

3.3 Quantum Efficiency and Photo-Luminescence

Further explanations of the fastest behaviour of the triple-cation device are related to the spectral response of the photodetectors. In Figure 5, we reported the responsivity ($\mathcal{R}$) of the three types of device; each curve is normalized with respect to the max measured value, to better appreciate the different spectral behaviour. Considering MAPI-1 as a reference of the responsivity, FAMA-2 maintains an equivalent dependence with respect to wavelength; even the enlargement in the detectable wavelength range (~50nm, till 800nm) due to the perovskite type, is practically negligible, since the emission spectrum of the CW used as source (reported in Figure 5) is zero over 750nm. Instead, the CsFAMA-3 shows a noteworthy increase in the responsivity, exactly in the spectral

region in which we have the maximum of the cool-white LED emission (the 'blue' one, with the peak at ~450nm, λ_{CW1}).

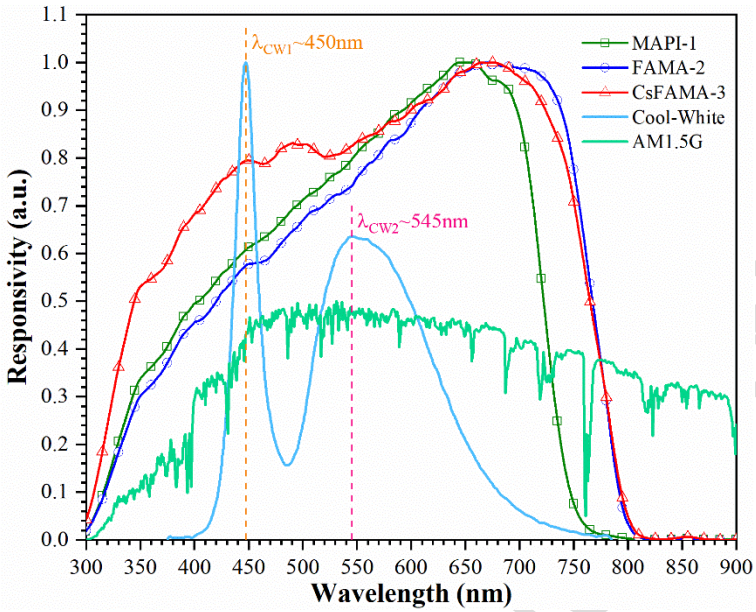

Figure 5. Normalized responsivity of the PVSK-PDs realized, compared to the emission spectrum of the Cool-White LED and solar spectrum (AM1.5G)

It has to be underlined that this larger responsivity around 450nm is in line with the increment of the absorption spectrum of triple-cation *(FA/MA/Cs)Pb(I/Br)* thin-films, with respect to the other ones, as showed in Figure 6. Neglecting the saturation of the absorption spectra (due to a limit of the spectrophotometer used), however the curve shape of the CsFAMA-3 rises faster than the others approaching 480nm (from highest wavelength); moreover, the behaviours are quite similar to others reported in literature [40]. This absorption increment of the blue part of the CW emission contributes significantly to the faster response of the device. In fact, a typical approach to speed up a VLC channel is the 'blue-pass' filtering of the optical signal from a CW source [10], since the fluorescent emission due to the YAG phosphors composing generally a white LED (the peak of this emission is at 545nm, λ_{CW2}) is perforce a slower optical signal, depending from the absorption of the blue portion and the consequent mechanisms of fluorescence. We therefore could interpret the larger responsivity to the blue emission like a "cut-off filter" of the YAG one. This mechanism is present only in the case of CsFAMA-3 based devices, thus boosting the time response for such kind of active material in the photodetector.

A further reason for the improved performance of CsFAMA-3 can be identified analysing the Photo-Luminescence (PL) response of the three different devices (Figure 6). The PL spectra, normalized with respect to the absolute maximum value measured, $PL(\lambda_{max})$, reveal that there is a stronger quenching in the case of CsFAMA-3, if compared to MAPI-1 and FAMA-2. This denotes that the CsFAMA-3 device presents a more efficient charge separation, and therefore an improved

collection of the photo-generated carriers [41]. We also observe that the relative PL intensities are consistent with the cut-off frequencies of all cases, since the quenching is expected to be inversely proportional to the charge separation efficiency (and consequently device speed). The $\lambda_{on\text{-}set}$ extimated for such curves (in the inset of Figure 6), together with the photo-luminescence parameters, are reported in Table 2.

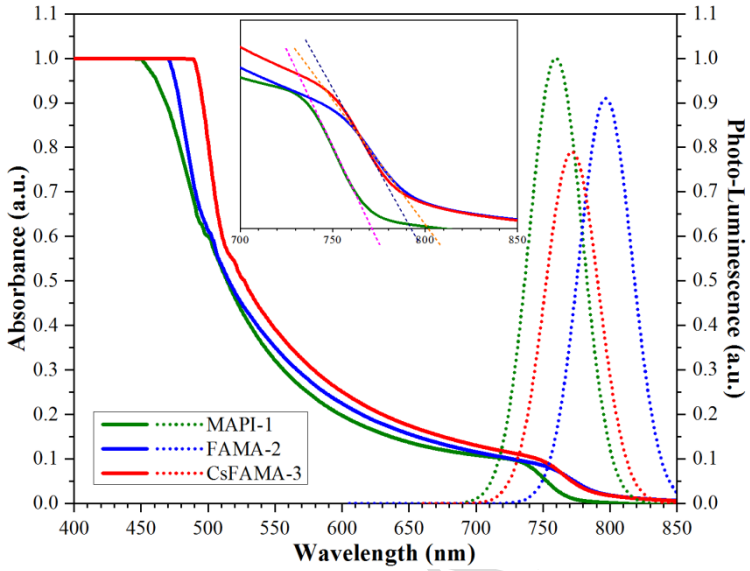

Figure 6. Absorbance (left) and Photo-luminescence (right) spectra obtained from the three different perovskite-based devices. For photo-luminescence, the curves are normalized with respect to the maximum peak value measured for the MAPI-1 (at 760nm). (Inset) On-set of the absorbance spectra of the three devices; the expected corresponding wavelengths ($\lambda_{on\text{-}set}$).

3.4 Time-dependent behaviour

Figure 7**Error! Reference source not found.** shows the output signal of the hybrid VLC system realized with the cool-white LED connected to a driver circuit as transmitter, and the receiver made with the best performing active material. The CsFAMA-3 perovskite-based photo-detector is connected to the TIA; the CW is directly modulated with an OOK (On-Off-Keying) based TTL (0↔3.3V) signal. As underlined before, it's possible to observe an initial increase in the output signal dynamic; this effect is due to the larger gain at certain frequencies, since the photodetector (natively a passive device) is connected to a TIA, which is an active component. In a realistic VLC system, the signal could be further optimized with the use of an appropriate filter/equalizer stage [4,10], but it was out of our purpose in this work. From the time-response curves of the three devices, the response time (τ_{resp}), equal to the sum of both rise- and fall-time, were estimated (see Table 2). Considering the state-of-the-art work of Bao *et al.* [42], in which is reported a rise-/fall-time of 20ns (best case) for a device active area of only 0.1mm^2, our CsFAMA-based photo-detector is completely in-line, since its response time of 1.633us is due to an active area 100 times greater. In fact, although the correlation between active area and geometrical capacitance (and consequently τ_{resp}) it's not completely linear,

however it's reasonable that a device of 10mm^2, realized following Bao's work, would lead to a response time of several microseconds.

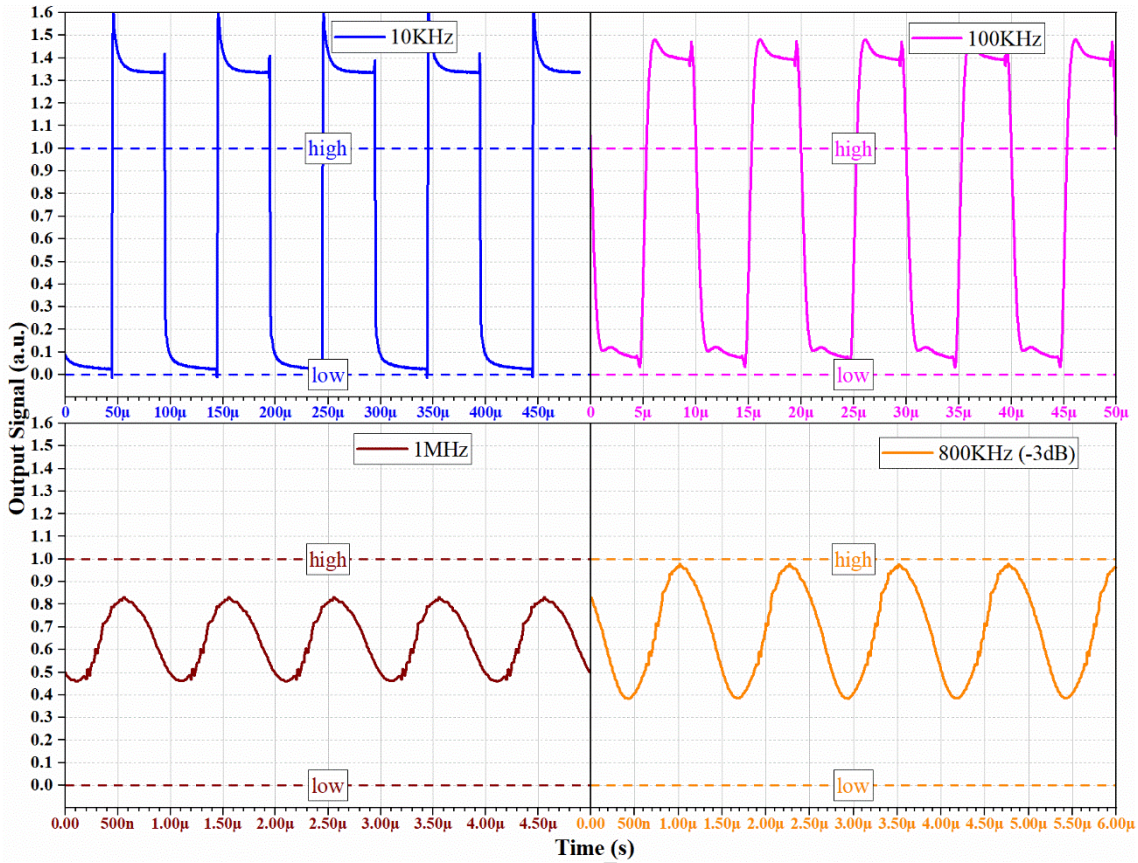

Figure 7. Output signal of the VLC receiver (PVSK-PD based on CsFAMA-3 and trans-impedance stage) under the Cool-White LED light stimulus at different frequencies. The CW is modulated directly with an electrical TTL (3.3V) at the frequency reported in the picture. The level states of the photodetector are defined by the steady-state illumination condition, dark (low, LED Off) or light (high, LED On).

In Figure 8 we reported also the Eye-Diagram of the VLC link. Differently from the output signal showed in Figure 7**Error! Reference source not found.**, the diagram is evaluated modulating the CW with a NRZ-PRBS (No-Return-to-Zero Pseudo-Random-Bit-Sequence). Eye diagram reveals that the perovskite-based photodetector realized with the CsFAMA-3 allows a robust optical link within a realistic scenario of data transmission. In Table 2 we report a summary of the principal parameters of the three perovskite-based devices.

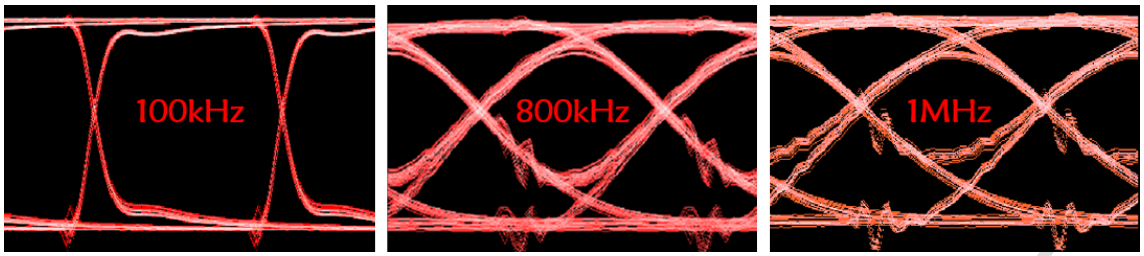

Figure 8. Eye-Diagram of the VLC channel realized with the CsFAMA-3 perovskite-based device, used as the photo-detector of the Rx (PVSK-PD + TIA).

Device	τ_{resp} ***(µs)***	$I_{on/off}$ ***(·10³)***	***λ (nm) @ $\mathfrak{R}_{max}$ (mA/W)***		***$\mathfrak{R}_{CW}$ (mA/W)***		***(Abs.) $\lambda_{on\text{-}set}$ (nm)***	***PL (a.u.)***		f_{off} ***(KHz)***
			λ	$\mathfrak{R}_{max}$	@ λ_{CW1}	@ λ_{CW2}		λ_{peak} *(nm)*	$PL(\lambda_{max})$	
MAPI-1	183	6.15	645	387	237	308	771	760	1	268
FAMA-2	2.532	2.55	670	372	215	276	802	796	0.91	584
CsFAMA-3	1.633	0.93	665	349	277	288	793	771	0.79	793

Table 2. Various parameters of the three PVSK-based photo-detector devices.

4. Conclusion

We have reported a VLC prototype link realized with a simple cool-white LED transmitter and an innovative hybrid-organic perovskite-based photovoltaic device, used in photo-detector mode (negative bias ~ -100mV). Three kinds of PVSK-PD were fabricated, following same steps in the fabrication procedure. All the materials are the same, with except of the perovskite layer, from single- to triple-cation type. Studying the properties of the different devices, we have observed a correlation between the classical parameters adopted in the evaluation of the performances of PVSK solar cells, such as hysteresis behaviour, and time dependent response of the PVSK photodetector. The reduced hysteresis delay of the triple cation based device is a clear indication of the improved PV performances as well as of the time dependent faster response. We have selected this device to realize and characterize a complete VLC link prototype. Generating a NRZ-PRBS for driving the CW with an OOK, we have reached a remarkable frequency bandwidth next to ~800KHz for the transmission of data in the VLC link.

Acknowledgments

We acknowledge the projects "PHLIGHT - Consolidate the Foundations" and "APOLO" from University of Rome "Tor Vergata", and "ORISHA" from ISCOM - Istituto Superiore delle Comunicazioni e delle Tecnologie dell'Informazione - Ministero dello Sviluppo Economico.

Reference

[1] L. Salamandra, G. Susanna, V. Attanasio, S. Penna, A. Reale, Organic Visible Light Communication, Atti Conf. GARR. Conferenza (2017) 79–85. doi:10.26314/GARR-Conf16-proceedings.

[2] H. Haas, LiFi is a paradigm-shifting 5G technology, Rev. Phys. 3 (2018) 26–31. doi:10.1016/j.revip.2017.10.001.

[3] J. Grubor, S. Randel, K.-D. Langer, J.W. Walewski, J.W. Grubor, J.; Randel, S.; Langer, K.D.; Walewski, Broadband Information Broadcasting Using LED-Based Interior Lighting, J. Light. Technol. 26 (2008) 3883–3892. doi:10.1109/JLT.2008.928525.

[4] D.C. O'Brien, L. Zeng, H. Le-Minh, G. Faulkner, J.W. Walewski, S. Randel, Visible light communications: Challenges and possibilities, in: 2008 IEEE 19th Int. Symp. Pers. Indoor Mob. Radio Commun., IEEE, 2008: pp. 1–5. doi:10.1109/PIMRC.2008.4699964.

[5] V. Sharma, S. Rajput, P.K. Sharma, Light fidelity (Li-Fi): An effective solution for data transmission, in: 2016: p. 020061. doi:10.1063/1.4942743.

[6] Li-Fi Applications, (n.d.). https://planetechusa.com/blog/li-fi-better-faster-and-greener-than-wi-fi-and-fiber-combined/.

[7] Z. Ghassemlooy, S. Arnon, M. Uysal, Z. Xu, J. Cheng, Emerging Optical Wireless Communications-Advances and Challenges, IEEE J. Sel. Areas Commun. 33 (2015) 1738–1749. doi:10.1109/JSAC.2015.2458511.

[8] Z. Ghassemlooy, L. Alves, S. Zvanovec, M.A. Khalighi, Visible Light Communications: Theory and Applications, Boca Raton: CRC Press (2017).

[9] J. Söderberg, Free Space Optics in the Czech Wireless Community: Shedding Some Light on the Role of Normativity for User-Initiated Innovations, Sci. Technol. Hum. Values. 36 (2011) 423–450. doi:10.1177/0162243910368398.

[10] H. Li, X. Chen, J. Guo, H. Chen, A 550 Mbit/s real-time visible light communication system

based on phosphorescent white light LED for practical high-speed low-complexity application, Opt. Express. 22 (2014) 27203. doi:10.1364/OE.22.027203.

[11] 802 IEEE Standard, (n.d.). https://standards.ieee.org/develop/project/802.15.7.html.

[12] A.-M. Cailean, M. Dimian, Impact of IEEE 802.15.7 Standard on Visible Light Communications Usage in Automotive Applications, IEEE Commun. Mag. (2017) 2–7. doi:10.1109/MCOM.2017.1600206CM.

[13] D. Tsonev, H. Chun, S. Rajbhandari, J.J.D. McKendry, S. Videv, E. Gu, M. Haji, S. Watson, A.E. Kelly, G. Faulkner, M.D. Dawson, H. Haas, D. O'Brien, A 3-Gb/s Single-LED OFDM-Based Wireless VLC Link Using a Gallium Nitride μLED, IEEE Photonics Technol. Lett. 26 (2014) 637–640. doi:10.1109/LPT.2013.2297621.

[14] H. Chun, S. Rajbhandari, G. Faulkner, D. Tsonev, E. Xie, J.J.D. McKendry, E. Gu, M.D. Dawson, D.C. O'Brien, H. Haas, LED Based Wavelength Division Multiplexed 10 Gb/s Visible Light Communications, J. Light. Technol. 34 (2016) 3047–3052. doi:10.1109/JLT.2016.2554145.

[15] H.J. Snaith, Perovskites: The Emergence of a New Era for Low-Cost, High-Efficiency Solar Cells, J. Phys. Chem. Lett. 4 (2013) 3623–3630. doi:10.1021/jz4020162.

[16] W. Chen, Y. Wu, Y. Yue, J. Liu, W. Zhang, X. Yang, H. Chen, E. Bi, I. Ashraful, M. Gratzel, L. Han, Efficient and stable large-area perovskite solar cells with inorganic charge extraction layers, Sci. (80-.). 350 (2015) 944–948. doi:10.1126/science.aad1015.

[17] W.S. Yang, J.H. Noh, N.J. Jeon, Y.C. Kim, S. Ryu, J. Seo, S.I. Seok, High-performance photovoltaic perovskite layers fabricated through intramolecular exchange, Sci. (80-.). 348 (2015) 1234–1237. doi:10.1126/science.aaa9272.

[18] X. Li, D. Bi, C. Yi, J.-D. Decoppet, J. Luo, S.M. Zakeeruddin, A. Hagfeldt, M. Gratzel, A vacuum flash-assisted solution process for high-efficiency large-area perovskite solar cells, Science (80-.). 353 (2016) 58–62. doi:10.1126/science.aaf8060.

[19] N.Y. Nia, F. Matteocci, L. Cina, A. Di Carlo, High-Efficiency Perovskite Solar Cell Based on Poly(3-Hexylthiophene): Influence of Molecular Weight and Mesoscopic Scaffold Layer, ChemSusChem. 10 (2017) 3854–3860. doi:10.1002/cssc.201700635.

[20] M.K. Sardashti, M. Zendehdel, N.Y. Nia, D. Karimian, M. Sheikhi, High Efficiency MAPbI 3 Perovskite Solar Cell Using a Pure Thin Film of Polyoxometalate as Scaffold Layer, ChemSusChem. 10 (2017) 3773–3779. doi:10.1002/cssc.201701027.

[21] A. Kojima, K. Teshima, Y. Shirai, T. Miyasaka, Organometal Halide Perovskites as Visible-Light Sensitizers for Photovoltaic Cells, J. Am. Chem. Soc. 131 (2009) 6050–6051. doi:10.1021/ja809598r.

[22] NREL Efficiency Chart, (n.d.). https://www.nrel.gov/pv/assets/images/efficiency-chart.png.

[23] C.-C. Chueh, C.-Z. Li, A.K.-Y. Jen, Recent progress and perspective in solution-processed Interfacial materials for efficient and stable polymer and organometal perovskite solar cells, Energy Environ. Sci. 8 (2015) 1160–1189. doi:10.1039/C4EE03824J.

[24] Z. Song, S.C. Watthage, A.B. Phillips, M.J. Heben, Pathways toward high-performance perovskite solar cells: review of recent advances in organo-metal halide perovskites for photovoltaic applications, J. Photonics Energy. 6 (2016) 022001. doi:10.1117/1.JPE.6.022001.

[25] J.-P. Correa-Baena, A. Abate, M. Saliba, W. Tress, T. Jesper Jacobsson, M. Grätzel, A. Hagfeldt, The rapid evolution of highly efficient perovskite solar cells, Energy Environ. Sci. 10 (2017) 710–727. doi:10.1039/C6EE03397K.

[26] K. Hwang, Y.-S. Jung, Y.-J. Heo, F.H. Scholes, S.E. Watkins, J. Subbiah, D.J. Jones, D.-Y. Kim, D. Vak, Toward Large Scale Roll-to-Roll Production of Fully Printed Perovskite Solar Cells, Adv. Mater. 27 (2015) 1241–1247. doi:10.1002/adma.201404598.

[27] B.J. Kim, D.H. Kim, Y.-Y. Lee, H.-W. Shin, G.S. Han, J.S. Hong, K. Mahmood, T.K. Ahn, Y.-C. Joo, K.S. Hong, N.-G. Park, S. Lee, H.S. Jung, Highly efficient and bending durable perovskite solar cells: toward a wearable power source, Energy Environ. Sci. 8 (2015) 916–921. doi:10.1039/C4EE02441A.

[28] J. Gong, S.B. Darling, F. You, Perovskite photovoltaics: life-cycle assessment of energy and environmental impacts, Energy Environ. Sci. 8 (2015) 1953–1968. doi:10.1039/C5EE00615E.

[29] N. Espinosa, L. Serrano-Luján, A. Urbina, F.C. Krebs, Solution and vapour deposited lead perovskite solar cells: Ecotoxicity from a life cycle assessment perspective, Sol. Energy Mater. Sol. Cells. 137 (2015) 303–310. doi:10.1016/j.solmat.2015.02.013.

[30] I. Celik, Z. Song, A.J. Cimaroli, Y. Yan, M.J. Heben, D. Apul, Life Cycle Assessment (LCA) of perovskite PV cells projected from lab to fab, Sol. Energy Mater. Sol. Cells. 156 (2016) 157–169. doi:10.1016/j.solmat.2016.04.037.

[31] J. Zhang, X. Gao, Y. Deng, Y. Zha, C. Yuan, Comparison of life cycle environmental impacts of different perovskite solar cell systems, Sol. Energy Mater. Sol. Cells. 166 (2017) 9–17. doi:10.1016/j.solmat.2017.03.008.

[32] K.P. Bhandari, J.M. Collier, R.J. Ellingson, D.S. Apul, Energy payback time (EPBT) and energy return on energy invested (EROI) of solar photovoltaic systems: A systematic review and meta-analysis, Renew. Sustain. Energy Rev. 47 (2015) 133–141. doi:10.1016/j.rser.2015.02.057.

[33] S. Casaluci, L. Cina, F. Matteocci, P. Lugli, A. Di Carlo, Fabrication and Characterization of Mesoscopic Perovskite Photodiodes, IEEE Trans. Nanotechnol. 15 (2016) 255–260. doi:10.1109/TNANO.2016.2517239.

[34] B.R. Sutherland, A.K. Johnston, A.H. Ip, J. Xu, V. Adinolfi, P. Kanjanaboos, E.H. Sargent, Sensitive, Fast, and Stable Perovskite Photodetectors Exploiting Interface Engineering, ACS Photonics. 2 (2015) 1117–1123. doi:10.1021/acsphotonics.5b00164.

[35] N. Yaghoobi Nia, M. Zendehdel, L. Cinà, F. Matteocci, A. Di Carlo, A crystal engineering approach for scalable perovskite solar cells and module fabrication: a full out of glove box procedure, J. Mater. Chem. A. 6 (2018) 659–671. doi:10.1039/C7TA08038G.

[36] B. Chen, M. Yang, S. Priya, K. Zhu, Origin of J – V Hysteresis in Perovskite Solar Cells, J. Phys. Chem. Lett. 7 (2016) 905–917. doi:10.1021/acs.jpclett.6b00215.

[37] D.A. Jacobs, Y. Wu, H. Shen, C. Barugkin, F.J. Beck, T.P. White, K. Weber, K.R. Catchpole, Hysteresis phenomena in perovskite solar cells: the many and varied effects of ionic accumulation, Phys. Chem. Chem. Phys. 19 (2017) 3094–3103. doi:10.1039/C6CP06989D.

[38] J. Carrillo, A. Guerrero, S. Rahimnejad, O. Almora, I. Zarazua, E. Mas-Marza, J. Bisquert, G. Garcia-Belmonte, Ionic Reactivity at Contacts and Aging of Methylammonium Lead Triiodide Perovskite Solar Cells, Adv. Energy Mater. 6 (2016) 1502246. doi:10.1002/aenm.201502246.

[39] T. Bu, X. Liu, Y. Zhou, J. Yi, X. Huang, L. Luo, J. Xiao, Z. Ku, Y. Peng, F. Huang, Y.-B. Cheng, J. Zhong, A novel quadruple-cation absorber for universal hysteresis elimination for high efficiency and stable perovskite solar cells, Energy Environ. Sci. 10 (2017) 2509–2515. doi:10.1039/C7EE02634J.

[40] Y. Sun, J. Peng, Y. Chen, Y. Yao, Z. Liang, Triple-cation mixed-halide perovskites: towards efficient, annealing-free and air-stable solar cells enabled by Pb(SCN)2 additive, Sci. Rep. 7 (2017) 46193. doi:10.1038/srep46193..

[41] M. Wang, Z. Zang, B. Yang, X. Hu, K. Sun, L. Sun, Performance improvement of perovskite solar cells through enhanced hole extraction: The role of iodide concentration gradient, Sol. Energy Mater. Sol. Cells. 185 (2018) 117–123. doi:10.1016/j.solmat.2018.05.025.

[42] C. Bao, J. Yang, S. Bai, W. Xu, Z. Yan, Q. Xu, J. Liu, High Performance and Stable All-Inorganic Metal Halide Perovskite-Based Photodetectors for Optical Communication Applications, Adv. Mater. 1803422 (2018) 1–8. doi:10.1002/adma.201803422.

Highlights

- We studied Perovskite-based photo-voltaic devices, but used as photo-detector.
- We varied the Perovskite type (single- to triple-cations) to evaluate device performance changing.
- We estimated the triple-cation Perovskite-based device as the best performer.
- We achieved an exciting cut-off frequency near 800KHz for the Perovskite photo-detector.

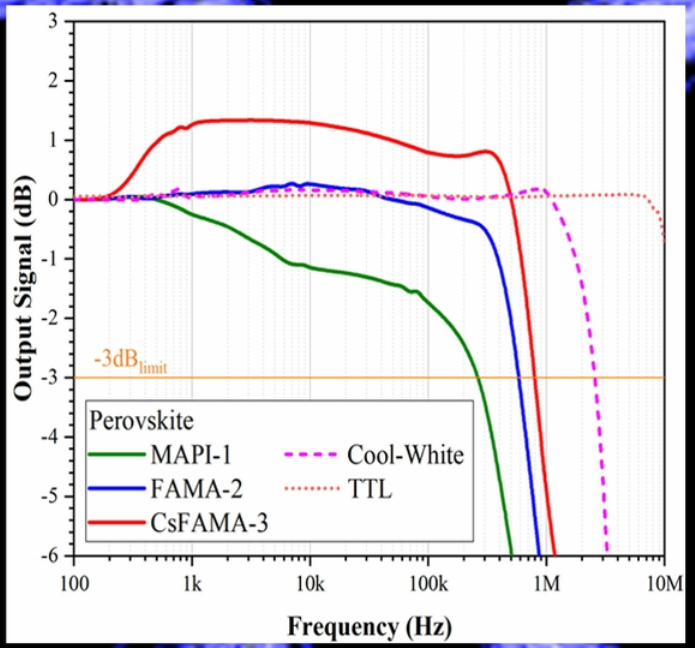
Output Signal (dB)
3
2
1
0
-1
-2
-3
-4
-5
-6
-3dB limit
Perovskite
MAPI-1
FAMA-2
CsFAMA-3
Cool-White
TTL
100
1k
10k
100k
1M
10M
Frequency (Hz)

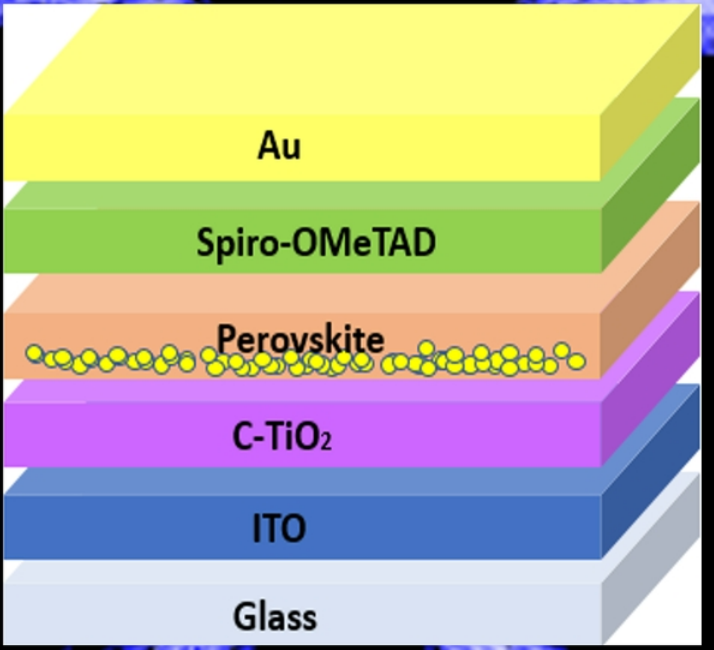
Au
Spiro-OMeTAD
Perovskite
C-TiO2
ITO
Glass